

Article

# Irreversibility Analysis of Hydromagnetic Casson Fluid Flow Through an Inclined Channel with Isothermal Boundary Conditions

Bernard Ejugu Njor <sup>1,\*</sup>, Ramoshweu Solomon Lebelo <sup>2</sup>  and Samuel Olumide Adesanya <sup>1,3</sup> <sup>1</sup> Department of Mathematics and Statistics, Redeemer's University, Ede 232101, Nigeria<sup>2</sup> Applied Physical Sciences Department, Vaal University of Technology, Private Bag X021, Vanderbijlpark 1911, South Africa; sollyl@vut.ac.za<sup>3</sup> Education Department, Vaal University of Technology, Private Bag X021, Vanderbijlpark 1911, South Africa

\* Correspondence: njorb@run.edu.ng

**Abstract:** Fluid flow along an inclined channel phenomenon is crucial in several geophysical, environmental, engineering, biological, and industrial processes, and in aerodynamics and hemodynamics. This present study examines the effect of a constant magnetic field on the entropy production rate in a steady flow of Casson fluid along an inclined heated channel. The governing equations for the flow of velocity, temperature, and entropy generation are formulated based on the Casson constitutive relations and thermodynamics' first and second laws. The exact solutions are constructed for the dimensionless equations and validated with previous results in the literature. The effects of various fluid parameters on the flow, heat transfer, and entropy production rate are conducted and reported graphically with adequate discussion. The impact of the Hartmann number parameter reveals a decrease in both flow velocity and entropy generation rate, meanwhile it also enhances the fluid temperature distribution across the inclined channel. An opposite trend is, however, observed with the Casson fluid parameter.

**Keywords:** hydromagnetic; inclined channel; entropy generation; Casson fluid**MSC:** 76-10

Academic Editor: Zhenquan Li

Received: 4 February 2025

Revised: 30 March 2025

Accepted: 1 April 2025

Published: 7 April 2025

**Citation:** Njor, B.E.; Lebelo, R.S.; Adesanya, S.O. Irreversibility Analysis of Hydromagnetic Casson Fluid Flow Through an Inclined Channel with Isothermal Boundary Conditions. *Mathematics* **2025**, *13*, 1208. <https://doi.org/10.3390/math13071208>

**Copyright:** © 2025 by the authors. Licensee MDPI, Basel, Switzerland. This article is an open access article distributed under the terms and conditions of the Creative Commons Attribution (CC BY) license (<https://creativecommons.org/licenses/by/4.0/>).

## 1. Introduction

Recently, remarkable progress has been made in studies on heat exchange and work potentials based on thermodynamics' first and second laws. These laws characterize the friction loss and heat exchange rate in a system [1,2]. Bejan [3] pioneered the entropy minimization in thermal designs. Over the years, this idea has been explored in investigations associated with irreversible energy losses in different fluid streams; for instance, Qayyum et al. [4] explored this approach in analyzing the dissipative Williamson fluid flow between two rotating disks with thermal radiation. The volumetric entropy and irreversibility ratio were accounted for in their analysis. Moreover, Khan et al. [5] investigated the minimization of entropy production of a viscous fluid flow and heat transportation through a thin needle. More recently, Yusuf et al. [6] examined the slip effect on the flow of a micropolar fluid, featuring the analysis of the second law of thermodynamics. Furthermore, other surveys are presented in references [7–9]. Obalalu et al. [10] examined aluminum alloy–titanium alloy/ethylene glycol hybrid nanofluid in the flow of non-Newtonian Oldroyd-B through a parabolic trough surface collector located in a solar water pump. Sanni et al. [11] studied entropy generation optimization in a couple stress fluid flows with variable viscosity and

aligned magnetic fields. Chen et al. [12] studied minimum entropy generation paths for generalized radiative heat transfer processes with heat leakage.

Real fluids exhibit non-Newtonian behavior due to their complex rheological properties. One of the subclasses of these liquids is Casson fluid, which behaves like a solid when shear stress lower than the yield stress is applied to the fluid, whereas it flows when shear stress greater than the yield stress is used. Examples include honey, tomato paste, and many more. Owing to the vast applications of this liquid, the magneto-hydrodynamics stream of Casson fluid has proved to be essential in machinery-related fields. The stream of Casson fluid through various geometries has been accounted for recently. Chui-On [13] investigates the influence of electro-osmotic Casson fluid flow in a slit microchannel. Mohyud-Din and Khan examined the squeezed flow of Casson fluid between parallel disks with nonlinear thermal radiation [14]. Ramesh and Devakar examined the exact solutions for the flow of Casson fluid over a slippery surface [15]. Recently, Atlas et al. [16] numerically investigated the irreversibility analysis on the transient flow of Casson fluid between equally distant plates with nonlinear heat and mass flux. In their study, Priam and Nasrin [17] numerically appraised the time-dependent peristaltic duct of Casson fluid by applying the finite element method of Galerkin's residual technique in obtaining a numerical solution. Nadeem et al. [18] analyzed a mathematical model of non-Newtonian Casson nanofluid, and Abbas et al. [19] investigated the application of heat and mass transfer to the convective flow of Casson fluids in a microchannel with the Caputo–Fabrizio derivative approach.

Numerous investigators have looked at studies on flow with a slantwise geometry. The analysis of fluid flow induced by physical forces such as gravity-driven flow with nonzero inclinations is being accounted for, particularly in the study of heat transfer, e.g., solar collective technology. Komurgoz et al. [20] employed a semi-analytical approach in investigating the entropy generation on a steady flow with non-isothermal walls. Hayat et al. [21] scrutinized the joint behavior of an inclined magnetic field and viscous dissipation on a peristaltic flow of Williamson fluid through an inclined symmetric channel. Dar and Elangovan examined the peristaltic flow of a micropolar fluid down an aligned channel with an aligned magnetic field [22]. Abbas et al. [23] studied the magnetohydrodynamic (MHD) flow and heat transfer of two immiscible fluids in an inclined channel. Lerisson et al. [24], Turkyilmazoglu [25], and Adesanya et al. [26] are among investigators who have recently examined the film flow and heat transfer down a slantwise substrate. Vaddemani et al. [27] addressed the effects of Soret on an unsteady free convection flow of viscous incompressible fluid through a porous medium with high porosity bounded by a vertical infinite moving plate under the influence of chemical reaction, heat source, and thermal diffusion. Hafez et al. [28] discussed the impact of heat and mass transfer on the MHD peristaltic flow of Casson fluid in a rotating inclined plane, and Mopuri et al. [29] also recently contributed by examining the characteristics of MHD Jeffery fluid on an inclined vertical plate.

Furthermore, Adesanya et al. [30] studied the steady flow of non-Newtonian fluids through an isothermal impervious wall, neglecting magnetic field interaction. Abbas et al. [31] studied the analysis of entropy generation on peristaltic phenomena of MHD in a diverging tube. Naz et al. [32] investigated the entropy generation optimization in MHD pseudoplastic fluid using a cylindrical (tube) channel and the Williamson fluid model. Jha and Yusuf [33] studied steady incompressible fluid flow through leaky walls without the effect of a magnetic field. Khalid et al. [34] studied an unsteady MHD free convection flow of Casson fluid over an oscillating vertical plate embedded in a porous medium. Awais et al. [35] studied heat and mass transfer phenomena for the dynamics of Casson fluid through a porous medium over a shrinking wall subject to Lorentz force and a heat source/sink. MHD free convective non-Newtonian Casson fluid flows over

an oscillating vertical plate were investigated by Prameela and his team [36]. Vishalakshi et al. [37] investigated the MHD Casson fluid flow with a porous medium. Just recently, Adel et al. [38] used the Adomian decomposition method (ADM) solution approach to investigate the behavior of a slippery nanofluid flowing over a permeable stretched sheet under the influence of MHD forces.

Despite the huge number of studies [1–38] around entropy generation, inclined channel, and Casson fluid, nothing much has been performed regarding monitoring the entropy generation around hydromagnetic Casson fluid flow down a heated inclined channel despite its huge applications in a good number of medical, industrial, and engineering applications. As a result, the main objective of this study is to extend the work by Jha and Yusuf [33] to its non-Newtonian case with a good number of applications in metallurgical and industrial engineering. In the following section, the model will be formulated based on Casson constitutive relation and magneto-hydrodynamics. In section three, the solution procedure will be described, in section four the graphical description of the solutions will be presented and explained, while section five concludes the study.

### 2. Problem Formulation

The steady flow of an electrically conducting Casson fluid down an inclined heated porous channel is considered in this work. The flow is assumed to be fully developed and the Cartesian coordinate is chosen in such a way that the  $x$ -axis aligns with the axial flow while the  $y$ -direction is taken perpendicular to it, as shown in the flow configuration (Figure 1). The constant wall temperatures are kept at  $T_1$  which is greater than the inlet condition for it to be of heat transfer interest, i.e.,  $T_1 > T_0$ .

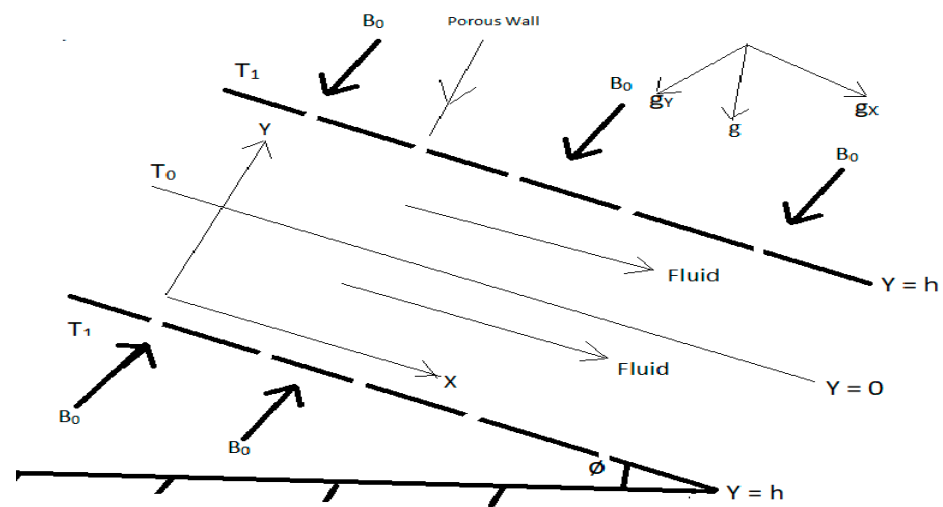


Figure 1. Flow configuration.

Neglecting the pressure drop since the gravitational force is much stronger, the equation governing the flow with constant fluid properties can be written as follows:

$$-\rho v_0 \frac{du'}{dy'} = \rho g \sin \phi + \mu \left( 1 + \frac{1}{\beta} \right) \frac{d^2 u'}{dy'^2} - \sigma B_0^2 u'. \tag{1}$$

The no-slip and the non-moving wall conditions are as follows:

$$u'(\pm h) = 0 \tag{2}$$

Since the walls are heated at constant temperature, the heat transfer due to temperature difference between the heated walls ( $T_1$ ) and the fluid inlet temperature ( $T_0$ ) during the

process is irreversible. As a result, the balanced energy equation for the heat flow can be written from the heat conservation law as follows, together with the inlet and the porous walls conditions:

$$\begin{aligned} \rho C_p \left( u' \frac{\partial T}{\partial x'} - v_0 \frac{\partial T}{\partial y'} \right) &= k \frac{\partial^2 T}{\partial y'^2}; \\ T(0, y) &= T_0, \quad T(x, \pm h) = T_w \end{aligned} \tag{3}$$

When heat is transferred from the heated walls to the core area of the channel containing viscous fluid it comes with entropy transfer at a molecular level due to the increase in the kinetic energy of the fluid. This disorderliness of the fluid particle is expected due to the non-inviscid nature of the fluid. Also, due to the fact that heat transfer to viscous fluid is an irreversible process, the decay in the work potential in the thermal system due to a non-negative entropy change as postulated in the second law can be written as follows:

$$\dot{S}_{gen} = \frac{k}{T_0^2} \left( \left( \frac{\partial T}{\partial x'} \right)^2 + \left( \frac{\partial T}{\partial y'} \right)^2 \right) + \frac{\mu}{T_0} \left( 1 + \frac{1}{\beta} \right) \left( \frac{du'}{dy'} \right)^2 + \frac{\sigma B_0^2 u'^2}{T_0} \tag{4}$$

As a consequence of the second law,  $\dot{S}_{gen} > 0$  implies that  $(k, \mu, \sigma) > 0$  must be strictly satisfied for (4) to make any sense in physics. The wall skin friction and the heat transfer rate are given by the following:

$$\tau_{xy} = \mu \left( 1 + \frac{1}{\beta} \right) \frac{du'}{dy'} \Big|_{y=-h}, \quad Nu_x = \frac{hq}{k(T_w - T_0)}; \quad q = -k \frac{dT'}{dy'} \Big|_{y=-h} \tag{5}$$

To make Equations (1)–(5) dimensionless, the following variables and parameters are used:

$$\begin{aligned} y &= \frac{y'}{h}, \quad x = \frac{\alpha \mu x'}{\rho g h^4 \sin \phi}, \quad u = \frac{\mu u'}{\rho g h^2 \sin \phi} = \frac{u'}{v_0}, \quad Ha^2 = \frac{\sigma B_0^2 h^2}{\mu}, \\ Pr &= \frac{v}{\alpha}, \quad \alpha = \frac{k}{\rho C_p}, \quad S = \frac{\rho v_0 h}{\mu}, \quad Ns = \frac{S_G h^2 T_0^2}{k(T_w - T_0)^2}, \quad Pe = \frac{\rho g h^3 \sin \phi}{\alpha \mu} \\ \theta &= \frac{T - T_0}{T_w - T_0}, \quad \Omega = \frac{T_w - T_0}{T_0}, \quad Br = Ec.Pr = \frac{\mu v_0^2}{k(T_w - T_0)}, \quad Ec = \frac{v_0^2}{C_p(T_w - T_0)}, \end{aligned} \tag{6}$$

The resulting boundary-value problems are given by the following:

$$\left. \begin{aligned} 0 &= 1 + \left( 1 + \frac{1}{\beta} \right) \frac{d^2 u}{dy^2} + S \frac{du}{dy} - Ha^2 u; & u(\pm 1) &= 0 \\ u \frac{\partial \theta}{\partial x} &= \frac{\partial^2 \theta}{\partial y^2} + Pr S \frac{\partial \theta}{\partial y}; & \theta(0, y) &= 0, \quad \theta(x, \pm 1) = 1 \end{aligned} \right\} \tag{7}$$

While the dimensionless skin friction and wall Nusselt number are given by the following:

$$SF = \mu \left( 1 + \frac{1}{\beta} \right) \frac{du}{dy} \Big|_{y=-1}, \quad Nu_x = - \frac{d\theta}{dy} \Big|_{y=-1} \tag{8}$$

With the (7) and (8) known, the positive definite total entropy produced along the heated inclined channel becomes the following:

$$\begin{aligned} Ns &= \left( \frac{1}{Pe^2} \left( \frac{\partial \theta}{\partial x} \right)^2 + \left( \frac{\partial \theta}{\partial y} \right)^2 \right) + \frac{Br}{\Omega} \left( \left( 1 + \frac{1}{\beta} \right) \left( \frac{du}{dy} \right)^2 + Ha^2 u^2 \right) \\ &= N_x + N_y + N_{FF} + N_{OH} \end{aligned} \tag{9}$$

where the first term in (9) represents the entropy generation due to heat transfer along the x-direction, the second term represents the entropy produced due to heat transfer along the y-coordinate, the third term is the entropy generated due to viscous fluid interaction, and the last term is the entropy produced due to electric heating effect of the transverse magnetic field (ohmic heating of the fluid).

Another important tool is the Bejan number, which is the ratio of heat transfer to the total entropy generated along the inclined heated channel, and is given as follows:

$$Be = \frac{\frac{1}{Pe^2} \left(\frac{\partial \theta}{\partial x}\right)^2 + \left(\frac{\partial \theta}{\partial y}\right)^2}{\left(\frac{1}{Pe^2} \left(\frac{\partial \theta}{\partial x}\right)^2 + \left(\frac{\partial \theta}{\partial y}\right)^2\right) + \frac{Br}{\Omega} \left(\left(1 + \frac{1}{\beta}\right) \left(\frac{du}{dy}\right)^2 + Ha^2 u^2\right)} \tag{10}$$

### 3. Method of Solution

The system of Equation (7) is not coupled; hence the solution for the non-homogeneous velocity field  $u(y)$  can be obtained by using the method of undetermined coefficient to arrive at, which is as follows:

$$u(y) = \frac{1}{Ha^2} + A_1 e^{my} + A_2 e^{ny} \tag{11}$$

Using (11) in the partial differential equation, then the separation of variables approach suggests that Equation (8) can be written as follows:

$$\frac{\partial \theta}{\partial x} = \frac{1}{u} \left(\frac{\partial^2 \theta}{\partial y^2} + PrS \frac{\partial \theta}{\partial y}\right) = \lambda \tag{12}$$

From (12), we obtain the following differential equations by separation of variables:

$$\left. \begin{aligned} \frac{\partial \theta}{\partial x} &= \lambda, \\ \frac{d^2 \theta}{dy^2} + PrS \frac{d\theta}{dy} - \lambda u &= 0. \end{aligned} \right\} \tag{13}$$

So that the nontrivial solution of (12) is assumed to be of the following form:

$$\theta(x, y) = \lambda x + \theta(y) \tag{14}$$

where  $\theta(y)$  satisfies

$$\theta(y) = -\frac{\lambda y}{Ha^2 PrS} + \frac{Ke^{PrSy}}{PrS} + L + \frac{\lambda A_1 e^{my}}{m(m - PrS)} + \frac{\lambda A_2 e^{ny}}{n(n - PrS)} \tag{15}$$

In view of (14) and (15) and the thermal boundary conditions, the exact solution for  $\theta(x, y)$  is given by the following:

$$\theta(x, y) = \frac{e^{m+n} (e^{2PrS} - 1) Ha^2 mn PrS (m - PrS) (n - PrS) x}{\xi(x, y)}$$

where

$$\xi(x, y) = e^n \left( e^{m+my} - e^{2m} - e^{m+2PrS+my} + e^{2PrS} + e^{PrS(1+y)} (e^{2m} - 1) \right) Ha^2 n PrS (n - PrS) A_1 + e^m m (m - PrS) \left( \begin{aligned} &e^n n (n - PrS) \left( 1 - 2e^{PrS(1+y)} - Ha^2 PrS x - y + e^{2PrS} (1 + Ha^2 PrS x + y) \right) \\ &- Ha^2 PrS \left( e^{2n} - e^{2PrS} + e^{n+ny} (e^{2PrS} - 1) - 2e^{n+PrS(1+y)} \text{ Sinh}(n) \right) A_2 \end{aligned} \right)$$

For values of  $A_1, A_2, m, n, L, K,$  and  $\lambda$  please see Appendix A on page 11–14.

### 4. Discussion of Results

In this section, the graphical examination of the exact solutions  $u(y), \theta(x, y)$  are presented here with emphasis on some important fluid parameters. The range of values

adopted in this study is based on the associated theoretical and experimental analysis reported in different literature.

Figures 2–5 examine the behavior of the magnetic field on profiles of the velocity, temperature, entropy generation, and Bejan number, respectively. Figure 2 shows that a rise in the magnetic field intensity parameter decreases the velocity profile due to increasing magnetic field induction and its retarding effect of fluid motion across the inclined channel.

Meanwhile, kinetic energy is generated from frictional interaction in the moving fluid layers due to increased bonding strength and fluid viscosity. As a result, fluid temperature is expected to rise, as shown in Figure 3. As seen in Figure 4, the entropy generation rate is reduced due to the decreasing effect of the Hartmann number ( $Ha$ ) on the velocity profile since inter-particle collision at the molecular level will decrease with decreasing flow velocity. From Figure 2, velocity decreases with an increasing magnetic field intensity parameter (Hartmann number). The fluid friction decreases accordingly. This is because a rise in magnetic field intensity parameter implies a reduction in viscosity. Moreover, in Figure 3,  $Ha$  has been represented as an increasing function of temperature. Therefore, the effect is seen in Figure 4, where  $Ha$  decreases the entropy generation rate with the heated inclined channel. Figure 4 suggests the dominance of heat transfer irreversibility over friction fluid irreversibility since the maximum is approximately one, which is only possible when  $\frac{Br}{\Omega} \approx 0$ . Therefore, the effect of the magnetic field intensity parameter on the irreversibility ratio is seen to be very weak. The magnitude of the entropy production significantly declines as the magnetic field intensity parameter increases. The influence of the parameter on the Bejan number is depicted in Figure 5. The Bejan number monitors the quantity of heat transfer irreversibility to the overall heat transfer by the fluid friction. The dominance of heat transfer to the irreversibility ratio is observed to have an increasing impact on the heated walls of the aligned channel. It gradually declines as it moves towards the center. However, the irreversibility due to heat transfer controls the flow system at the heated walls.

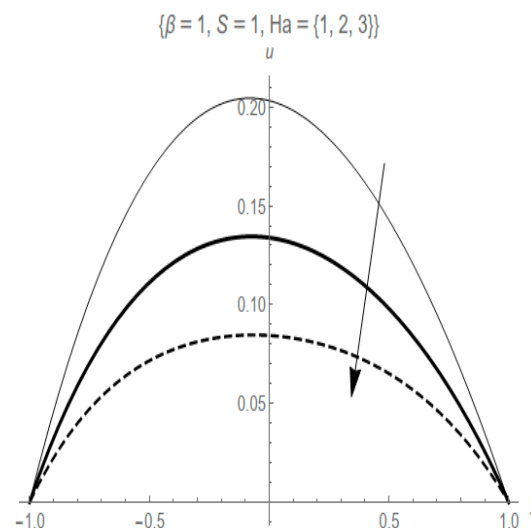


Figure 2. Velocity profile for  $\{Ha = 1, 2, 3\}$ .

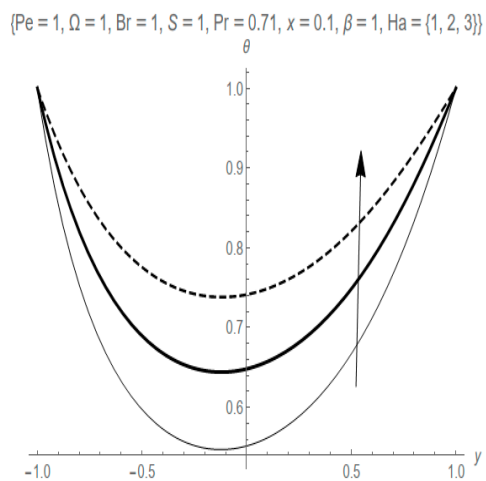


Figure 3. Temperature profile for {Ha = 1, 2, 3}.

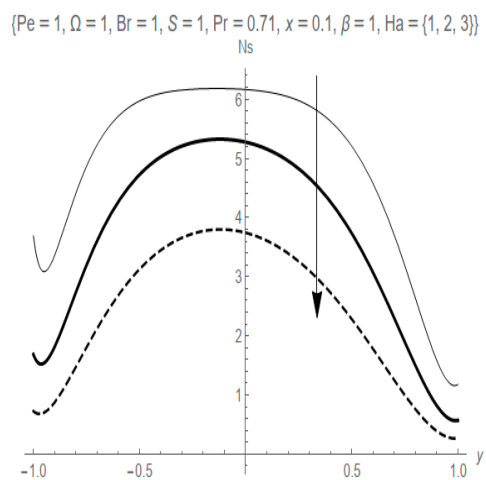


Figure 4. Entropy generation profile for {Ha = 1, 2, 3}.

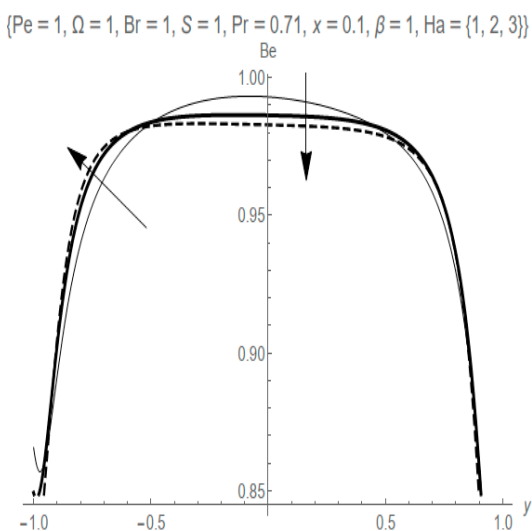


Figure 5. Bejan number for {Ha = 1, 2, 3}.

The response of the Casson fluid parameter against the profile of velocity, temperature, rate of entropy generation, and the irreversibility ratio is established in Figures 6–9. The result in Figure 6 depicts that increasing the value of the Casson fluid parameter upsurges the velocity profile. This reveals that the magnitude of the non-Newtonian fluid motion

is lower than that of the viscous fluid’s velocity. An increase in  $\beta$  leads to an increase in the velocity maximum, which approaches the Newtonian limit. Figure 7 describes the response of temperature distribution to variation in the Casson fluid parameter. Here, an increase in the Casson fluid parameter causes a decrease in the temperature distribution throughout the channel, whereas the fluid velocity is enhanced with increasing values of  $\beta$ . As displayed in Figure 8, an enhancement in the Casson fluid parameter improves the entropy production rate. The viscous dissipation and ohmic heating contribution are more excellent at the walls than heat transfer. This is a result of an increase in velocity in Figure 6 and a decrease in temperature in Figure 7. The fluid friction irreversibility contribution to heat transfer irreversibility is slightly noticed at both ends of the heated walls. In contrast, an enhanced value in the Casson fluid parameter influences the dominance of fluid friction over heat transfer irreversibility at the middle of the channel, as shown in Figure 9. The Bejan number attains a maximum of one when the heat transfer irreversibility effect is dominant. There is no effect on friction fluid irreversibility or ohmic heating. It reaches a value of 0.5 when the impact of heat transfer irreversibility is equal to the effect of friction fluid irreversibility and ohmic heating. In contrast, the value tends towards zero when the effect of the combination of friction fluid irreversibility and ohmic heating dominates over heat transfer irreversibility. This implies that heat transfer irreversibility is more substantial at the core area of the channel.

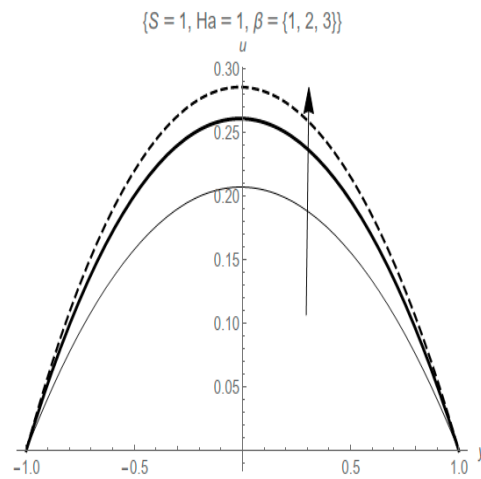


Figure 6. Velocity profile for  $\{\beta = 1, 2, 3\}$ .

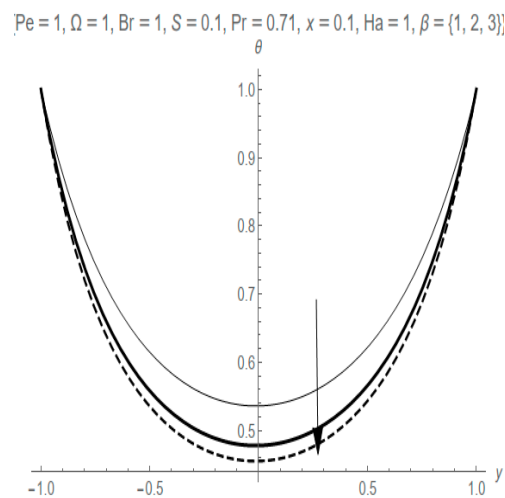


Figure 7. Temperature profile for  $\{\beta = 1, 2, 3\}$ .

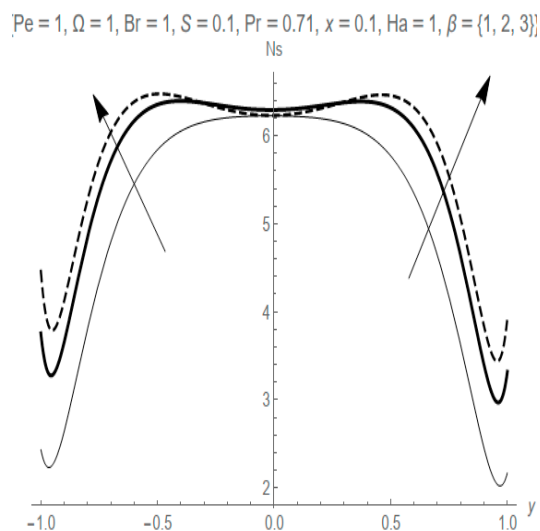


Figure 8. Entropy generation profile for  $\{\beta = 1, 2, 3\}$ .

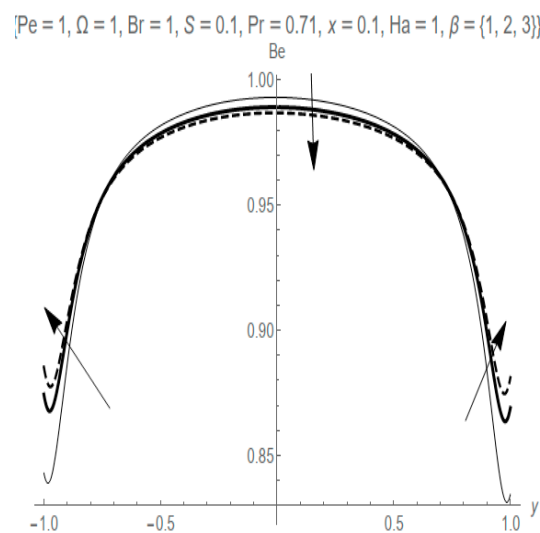


Figure 9. Bejan number for  $\{\beta = 1, 2, 3\}$ .

### 5. Conclusions

In the present study, analytical simulation for MHD Casson fluid flow down an inclined channel with isothermal boundary conditions was examined. Exact solution of dimensionless equations are obtained in a straightforward manner and are used to compute the entropy generation rate and irreversibility ratio. Some significant outcomes of the current study are highlighted below:

- The Casson fluid parameter increases fluid flow velocity and entropy generation rate while it decreases the fluid temperature profile.
- The Hartmann number parameter decreases fluid flow velocity and entropy generation rate while it increases the fluid temperature profile.
- The Casson fluid parameter causes the fluid friction irreversibility to dominate at the ends of the wall but weakens the dominance at the core area of the channel.
- The Hartmann number parameter influences the dominance of heat transfer irreversibility at the heated walls and decreases the dominance at the center of the channel.

**Author Contributions:** Conceptualization, S.O.A.; Methodology, S.O.A.; Validation, B.E.N.; Formal analysis, B.E.N.; Investigation, R.S.L.; Resources, R.S.L.; Writing—original draft, B.E.N.; Supervision,

S.O.A.; Funding acquisition, R.S.L. All authors have read and agreed to the published version of the manuscript.

**Funding:** This research received no external funding.

**Data Availability Statement:** Data will be made available on request.

**Conflicts of Interest:** The authors declare no conflict of interest.

### Nomenclature

$(v_0, \rho)$	constant vertical velocity and fluid density,
$(u', \phi)$	axial velocity and inclination angle,
$(\mu, \beta)$	dynamic viscosity, Casson material
$(\sigma, B_0)$	electrical conductivity and constant magnetic induction.
$(g, k)$	gravitational acceleration and thermal conductivity
$(C_p, T)$	specific heat capacity, fluid temperature
$(x', y')$	cartesian coordinate
$(x, y)$	dimensionless cartesian coordinate
$(T_0, T_1)$	fluid and heated wall temperatures.
$(u, \theta)$	dimensionless velocity and temperature
$(Ha, S)$	magnetic field and suction/injection
$(Pr, \alpha)$	Prandtl number and kinematic viscosity
$(Pe, Ec)$	Peclet and Eckert numbers
$(\Omega, Br)$	temperature difference and Brinkman number
Ns	dimensionless entropy generation rate
Be	Bejan Number (irreversibility)

### Appendix A

Where

$$A_1 = \frac{e^m (e^{2n} - 1)}{(e^{2m} - e^{2n})Ha^2}$$

$$A_2 = \frac{e^n (e^{2m} - 1)}{(e^{2n} - e^{2m})Ha^2}$$

$$m = \frac{1}{2} \left[ -\frac{S\beta}{1 + \beta} - \frac{\sqrt{\beta} \sqrt{4Ha^2 + 4Ha^2\beta + S^2\beta}}{1 + \beta} \right]$$

$$n = \frac{1}{2} \left[ -\frac{S\beta}{1 + \beta} + \frac{\sqrt{\beta} \sqrt{4Ha^2 + 4Ha^2\beta + S^2\beta}}{1 + \beta} \right]$$

$$L = - \left( \left( \left( -\frac{y}{\text{Ha}^2 \text{PrS}} - \frac{e^{my} A_1}{m(m+\text{PrS})} - \frac{e^{ny} A_2}{n(n+\text{PrS})} \right) \left( \frac{e^{-\text{PrSy}} \left( \frac{1}{\text{Ha}^2 \text{PrS}} + x + \frac{e^m A_1}{m(m+\text{PrS})} + \frac{e^n A_2}{n(n+\text{PrS})} \right)}{\text{PrS}} \right) \right. \right. \\ \left. \left. - \frac{e^{-\text{PrS}} \left( \frac{y}{\text{Ha}^2 \text{PrS}} + \frac{e^{my} A_1}{m(m+\text{PrS})} + \frac{e^{ny} A_2}{n(n+\text{PrS})} \right)}{\text{PrS}} \right) \right) \\ - \left( -\frac{y}{\text{Ha}^2 \text{PrS}} - \frac{e^{my} A_1}{m(m+\text{PrS})} - \frac{e^{ny} A_2}{n(n+\text{PrS})} \right) \left( \frac{e^{-\text{PrSy}} \left( -\frac{1}{\text{Ha}^2 \text{PrS}} + x + \frac{e^{-m} A_1}{m(m+\text{PrS})} + \frac{e^{-n} A_2}{n(n+\text{PrS})} \right)}{\text{PrS}} \right) \\ - \frac{e^{\text{PrS}} \left( \frac{y}{\text{Ha}^2 \text{PrS}} + \frac{e^{my} A_1}{m(m+\text{PrS})} + \frac{e^{ny} A_2}{n(n+\text{PrS})} \right)}{\text{PrS}} \left. \right) \\ / \left( \left( \frac{1}{\text{Ha}^2 \text{PrS}} - x + \frac{y}{\text{Ha}^2 \text{PrS}} - \frac{e^{-m} A_1}{m(m+\text{PrS})} + \frac{e^{my} A_1}{m(m+\text{PrS})} - \frac{e^{-n} A_2}{n(n+\text{PrS})} \right. \right. \\ \left. \left. + \frac{e^{ny} A_2}{n(n+\text{PrS})} \right) \left( \frac{e^{-\text{PrSy}} \left( \frac{1}{\text{Ha}^2 \text{PrS}} + x + \frac{e^m A_1}{m(m+\text{PrS})} + \frac{e^n A_2}{n(n+\text{PrS})} \right)}{\text{PrS}} \right) \right. \\ \left. - \frac{e^{-\text{PrS}} \left( \frac{y}{\text{Ha}^2 \text{PrS}} + \frac{e^{my} A_1}{m(m+\text{PrS})} + \frac{e^{ny} A_2}{n(n+\text{PrS})} \right)}{\text{PrS}} \right) \\ - \left( -\frac{1}{\text{Ha}^2 \text{PrS}} - x + \frac{y}{\text{Ha}^2 \text{PrS}} - \frac{e^m A_1}{m(m+\text{PrS})} + \frac{e^{my} A_1}{m(m+\text{PrS})} - \frac{e^n A_2}{n(n+\text{PrS})} \right. \\ \left. + \frac{e^{ny} A_2}{n(n+\text{PrS})} \right) \left( \frac{e^{-\text{PrSy}} \left( -\frac{1}{\text{Ha}^2 \text{PrS}} + x + \frac{e^{-m} A_1}{m(m+\text{PrS})} + \frac{e^{-n} A_2}{n(n+\text{PrS})} \right)}{\text{PrS}} \right) \\ \left. - \frac{e^{\text{PrS}} \left( \frac{y}{\text{Ha}^2 \text{PrS}} + \frac{e^{my} A_1}{m(m+\text{PrS})} + \frac{e^{ny} A_2}{n(n+\text{PrS})} \right)}{\text{PrS}} \right) \right) \right)$$

$$K = - \left( \left( e^{\text{PrS}+\text{PrSy}\text{PrS}} \left( 2e^{m+n} m^2 n^2 + 2e^{m+n} m^2 n \text{PrS} + 2e^{m+n} mn^2 \text{PrS} + 2e^{m+n} mn \text{Pr}^2 S^2 \right. \right. \right. \\ \left. \left. - e^n \text{Ha}^2 n^2 \text{PrS} A_1 + e^{2m+n} \text{Ha}^2 n^2 \text{PrS} A_1 - e^n \text{Ha}^2 n \text{Pr}^2 S^2 A_1 \right. \right. \\ \left. \left. + e^{2m+n} \text{Ha}^2 n \text{Pr}^2 S^2 A_1 - e^m \text{Ha}^2 m^2 \text{PrS} A_2 + e^{m+2n} \text{Ha}^2 m^2 \text{PrS} A_2 \right. \right. \\ \left. \left. - e^m \text{Ha}^2 m \text{Pr}^2 S^2 A_2 + e^{m+2n} \text{Ha}^2 m \text{Pr}^2 S^2 A_2 \right) \right) / \left( -2e^{m+n+\text{PrS}} m^2 n^2 \right. \\ \left. + e^{m+n+\text{PrSy}} m^2 n^2 + e^{m+n+2\text{PrS}+\text{PrSy}} m^2 n^2 - 2e^{m+n+\text{PrS}} m^2 n \text{PrS} \right. \\ \left. + e^{m+n+\text{PrSy}} m^2 n \text{PrS} + e^{m+n+2\text{PrS}+\text{PrSy}} m^2 n \text{PrS} - 2e^{m+n+\text{PrS}} mn^2 \text{PrS} \right. \\ \left. + e^{m+n+\text{PrSy}} mn^2 \text{PrS} + e^{m+n+2\text{PrS}+\text{PrSy}} mn^2 \text{PrS} - 2e^{m+n+\text{PrS}} mn \text{Pr}^2 S^2 \right. \\ \left. + e^{m+n+\text{PrSy}} mn \text{Pr}^2 S^2 + e^{m+n+2\text{PrS}+\text{PrSy}} mn \text{Pr}^2 S^2 - e^{m+n+\text{PrSy}} \text{Ha}^2 m^2 n^2 \text{PrS} x \right. \\ \left. + e^{m+n+2\text{PrS}+\text{PrSy}} \text{Ha}^2 m^2 n^2 \text{PrS} x - e^{m+n+\text{PrSy}} \text{Ha}^2 m^2 n \text{Pr}^2 S^2 x \right. \\ \left. + e^{m+n+2\text{PrS}+\text{PrSy}} \text{Ha}^2 m^2 n \text{Pr}^2 S^2 x - e^{m+n+\text{PrSy}} \text{Ha}^2 mn \text{Pr}^3 S^3 x \right. \\ \left. + e^{m+n+2\text{PrS}+\text{PrSy}} \text{Ha}^2 mn \text{Pr}^3 S^3 x + e^{m+n+\text{PrSy}} m^2 n^2 y - e^{m+n+2\text{PrS}+\text{PrSy}} m^2 n^2 y \right. \\ \left. + e^{m+n+\text{PrSy}} m^2 n \text{PrSy} - e^{m+n+2\text{PrS}+\text{PrSy}} m^2 n \text{PrSy} + e^{m+n+\text{PrSy}} mn^2 \text{PrSy} \right. \\ \left. - e^{m+n+2\text{PrS}+\text{PrSy}} mn^2 \text{PrSy} + e^{m+n+\text{PrSy}} mn \text{Pr}^2 S^2 y \right. \\ \left. - e^{m+n+2\text{PrS}+\text{PrSy}} mn \text{Pr}^2 S^2 y + e^{n+\text{PrS}} \text{Ha}^2 n^2 \text{PrS} A_1 \text{Ha}^2 n^2 \text{PrS} A_1 \right. \\ \left. + e^{2m+n+2\text{PrS}+\text{PrSy}} \text{Ha}^2 n^2 \text{PrS} A_1 + e^{m+n+my+\text{PrSy}} \text{Ha}^2 n^2 \text{PrS} A_1 \right. \\ \left. - e^{2m+n+\text{PrS}} \text{Ha}^2 n^2 \text{PrS} A_1 - e^{n+\text{PrSy}} - e^{m+n+2\text{PrS}+my+\text{PrSy}} \text{Ha}^2 n^2 \text{PrS} A_1 \right. \\ \left. + e^{n+\text{PrS}} \text{Ha}^2 n \text{Pr}^2 S^2 A_1 - e^{2m+n+\text{PrS}} \text{Ha}^2 n \text{Pr}^2 S^2 A_1 - e^{n+\text{PrSy}} \text{Ha}^2 n \text{Pr}^2 S^2 A_1 \right. \\ \left. + e^{2m+n+2\text{PrS}+\text{PrSy}} \text{Ha}^2 n \text{Pr}^2 S^2 A_1 + e^{m+n+my+\text{PrSy}} \text{Ha}^2 n \text{Pr}^2 S^2 A_1 \right. \\ \left. - e^{m+n+2\text{PrS}+my+\text{PrSy}} \text{Ha}^2 n \text{Pr}^2 S^2 A_1 + e^{m+\text{PrS}} \text{Ha}^2 m^2 \text{PrS} A_2 \right. \\ \left. - e^{m+2n+\text{PrS}} \text{Ha}^2 m^2 \text{PrS} A_2 - e^{m+\text{PrSy}} \text{Ha}^2 m^2 \text{PrS} A_2 \right. \\ \left. + e^{m+2n+2\text{PrS}+\text{PrSy}} \text{Ha}^2 m^2 \text{PrS} A_2 + e^{m+n+ny+\text{PrSy}} \text{Ha}^2 m^2 \text{PrS} A_2 \right. \\ \left. - e^{m+n+2\text{PrS}+ny+\text{PrSy}} \text{Ha}^2 m^2 \text{PrS} A_2 + e^{m+\text{PrS}} \text{Ha}^2 m \text{Pr}^2 S^2 A_2 \right. \\ \left. - e^{m+2n+\text{PrS}} \text{Ha}^2 m \text{Pr}^2 S^2 A_2 - e^{m+\text{PrSy}} \text{Ha}^2 m \text{Pr}^2 S^2 A_2 \right. \\ \left. + e^{m+2n+2\text{PrS}+\text{PrSy}} \text{Ha}^2 m \text{Pr}^2 S^2 A_2 + e^{m+n+ny+\text{PrSy}} \text{Ha}^2 m \text{Pr}^2 S^2 A_2 \right. \\ \left. - e^{m+n+2\text{PrS}+ny+\text{PrSy}} \text{Ha}^2 m \text{Pr}^2 S^2 A_2 \right) \right)$$

$$\lambda = \left( (-e^{m+n+PrSy} + e^{m+n+2PrS+PrSy})Ha^2mnPrS(m + PrS)(n + PrS) \right) / \left( -2e^{m+n+PrS}m^2n^2 + e^{m+n+PrSy}m^2n^2 + e^{m+n+2PrS+PrSy}m^2n^2 - 2e^{m+n+PrS}m^2nPrS + e^{m+n+PrSy}m^2nPrS + e^{m+n+2PrS+PrSy}m^2nPrS - 2e^{m+n+PrS}mn^2PrS + e^{m+n+PrSy}mn^2PrS + e^{m+n+2PrS+PrSy}mn^2PrS - 2e^{m+n+PrS}mnPr^2S^2 + e^{m+n+PrSy}mnPr^2S^2 + e^{m+n+2PrS+PrSy}mnPr^2S^2 - e^{m+n+PrSy}Ha^2m^2n^2PrSx + e^{m+n+2PrS+PrSy}Ha^2m^2n^2PrSx - e^{m+n+PrSy}Ha^2m^2nPr^2S^2x + e^{m+n+2PrS+PrSy}Ha^2m^2nPr^2S^2x - e^{m+n+PrSy}Ha^2mn^2Pr^2S^2x + e^{m+n+2PrS+PrSy}Ha^2mn^2Pr^2S^2x - e^{m+n+PrSy}Ha^2mnPr^3S^3x + e^{m+n+2PrS+PrSy}Ha^2mnPr^3S^3x + e^{m+n+PrSy}m^2n^2y - e^{m+n+2PrS+PrSy}m^2n^2y + e^{m+n+PrSy}m^2nPrSy - e^{m+n+2PrS+PrSy}m^2nPrSy + e^{m+n+PrSy}mn^2PrSy - e^{m+n+2PrS+PrSy}mn^2PrSy + e^{m+n+PrSy}mnPr^2S^2y - e^{m+n+2PrS+PrSy}mnPr^2S^2y + e^{n+PrS}Ha^2n^2PrSA_1 - e^{2m+n+PrS}Ha^2n^2PrSA_1 - e^{n+PrSy}Ha^2n^2PrSA_1 + e^{2m+n+2PrS+PrSy}Ha^2n^2PrSA_1 + e^{m+n+my+PrSy}Ha^2n^2PrSA_1 - e^{m+n+2PrS+my+PrSy}Ha^2n^2PrSA_1 + e^{n+PrS}Ha^2nPr^2S^2A_1 - e^{2m+n+PrS}Ha^2nPr^2S^2A_1 - e^{n+PrSy}Ha^2nPr^2S^2A_1 + e^{2m+n+2PrS+PrSy}Ha^2nPr^2S^2A_1 + e^{m+n+my+PrSy}Ha^2nPr^2S^2A_1 - e^{m+n+2PrS+my+PrSy}Ha^2nPr^2S^2A_1 + e^{m+PrS}Ha^2m^2PrSA_2 - e^{m+2n+PrS}Ha^2m^2PrSA_2 - e^{m+PrSy}Ha^2m^2PrSA_2 + e^{m+2n+2PrS+PrSy}Ha^2m^2PrSA_2 + e^{m+n+ny+PrSy}Ha^2m^2PrSA_2 - e^{m+n+2PrS+ny+PrSy}Ha^2m^2PrSA_2 + e^{m+PrS}Ha^2mPr^2S^2A_2 - e^{m+2n+PrS}Ha^2mPr^2S^2A_2 - e^{m+PrSy}Ha^2mPr^2S^2A_2 + e^{m+2n+2PrS+PrSy}Ha^2mPr^2S^2A_2 + e^{m+n+ny+PrSy}Ha^2mPr^2S^2A_2 - e^{m+n+2PrS+ny+PrSy}Ha^2mPr^2S^2A_2 \right)$$

## References

1. Bejan, A. *Entropy Generation Through Heat and Fluid Flow*; Wiley: New York, NY, USA, 1982.
2. Bejan, A. A study of entropy generation in fundamental convective heat-transfer. *J. Heat Transf.* **1979**, *101*, 718–725.
3. Bejan, A. Second-law analysis in heat transfer and thermal design. *Adv. Heat Transf.* **1982**, *15*, 1–58.
4. Qayyum, S.; Khan, M.I.; Hayat, T.; Alsaedi, A.; Tamoor, M. Entropy generation in dissipative flow of Williamson fluid between two rotating disks. *Int. J. Heat Mass. Transf.* **2018**, *127*, 933–942.
5. Khan, M.W.A.; Khan, M.I.; Hayat, T.; Alsaedi, A. Entropy generation minimization (EGM) of nanofluid flow by a thin moving needle with nonlinear thermal radiation. *Phys. B Condens. Matter* **2018**, *534*, 113–119.
6. Yusuf, T.A.; Naveen Kumar, R.; Prasannakumara, B.C.; Adesanya, S.O. Irreversibility analysis in micropolar fluid film along an incline porous substrate with slip effects. *Int. Commun. Heat Mass. Transf.* **2021**, *126*, 105357.
7. Rehman, A.U.; Mehmood, R.; Nadeem, S. Entropy analysis of radioactive rotating nanofluid with thermal slip. *Appl. Therm. Eng.* **2017**, *112*, 832–840. [[CrossRef](#)]
8. Eegunjobi, A.S.; Makinde, O.D. Irreversibility analysis of hydromagnetic flow of couple stress fluid with radiative heat in a channel filled with a porous medium. *Results Phys.* **2017**, *7*, 459–469.
9. Yusuf, T.; Mabood, F. Slip Effects and Entropy generation on inclined MHD flow of Williamson fluid through a permeable wall with chemical reaction via DTM. *Math. Model. Eng. Probl.* **2020**, *7*, 1–9. [[CrossRef](#)]
10. Obalalu, A.M.; Memon, M.A.; Saleem, S.; Abbas, A.; Olayemi, O.A.; Ali, M.R.; Sadat, R.; Hendy, A.S. Thermal performance of Oldroyd-B hybrid nanofluid in solar energy-based water pumping systems and entropy generation minimization. *Case Stud. Therm. Eng.* **2023**, *51*, 103476. [[CrossRef](#)]
11. Saini, G.; Hanumagowda, B.N.; Mulki, H.; Raju, S.S.K.; Varma, S.V.K.; Barghout, K.; Murshid, N.; Al-Kouz, W. Entropy generation optimization in couple stress fluid flow with variable viscosity and aligned magnetic field. *Sustainability* **2023**, *15*, 2493. [[CrossRef](#)]
12. Chen, L.; Xia, S.; Shi, S. Minimum entropy generation paths for generalized radiative heat transfer processes with heat leakage. *Results Eng.* **2024**, *21*, 101759. [[CrossRef](#)]
13. Ng, C.-O. Combined pressure-driven and electroosmotic flow of Casson fluid through a slit microchannel. *J. Non-Newton. Fluid Mech.* **2013**, *198*, 1–9. [[CrossRef](#)]
14. Mohyud-Din, S.T.; Khan, S.I. Nonlinear radiation effects on squeezing flow of a Casson fluid between parallel disks. *Aerosp. Sci. Technol.* **2016**, *48*, 186–192. [[CrossRef](#)]

15. Ramesh, K.; Devakar, M. Some analytical solutions for flows of Casson fluid with slip boundary conditions. *Ain Shams Eng. J.* **2015**, *6*, 967–975. [[CrossRef](#)]
16. Atlas, M.; Hussain, S.; Sagheer, M. Entropy generation and unsteady Casson fluid flow squeezing between two parallel plates subject to Cattaneo-Christov heat and mass flux. *Eur. Phys. J. Plus* **2019**, *134*, 33. [[CrossRef](#)]
17. Shadman Sakib, P.; Nasrin, R. Numerical appraisal of time-dependent peristaltic duct flow using Casson fluid. *Int. J. Mech. Sci.* **2022**, *233*, 107676. [[CrossRef](#)]
18. Nadeem, S.; Ishtiaq, B.; Hamida, M.B.B.; Almutairi, S.; Ghazwani, H.A.; Eldin, S.M.; Al-Shafay, A.S. Reynolds nanofluid model for Casson fluid flow conveying exponential nanoparticles through a slandering sheet. *Sci. Rep.* **2023**, *13*, 1953. [[CrossRef](#)]
19. Abbas, S.; Nisa, Z.U.; Nazar, M.; Amjad, M.; Ali, H.; Jan, A.Z. Application of heat and mass transfer to convective flow of Casson fluid in a microchannel with Caputo-Fabrizio derivative approach. *Arab. J. Sci. Eng.* **2024**, *49*, 1275–1286. [[CrossRef](#)]
20. Komurgoz, G.; Arikoglu, A.; Turker, E.; Ozkol, I. Second-law analysis for an inclined channel containing porous-clear fluid layers by using the differential transform method. *Numer. Heat Transf. Part. A* **2010**, *57*, 603–623. [[CrossRef](#)]
21. Hayat, T.; Shahida, B.; Rafiq, M.; Alsaedi, A.; Abbasi, F.M. Effect of an inclined magnetic field on peristaltic flow of Williamson fluid in an inclined channel with convective conditions. *J. Magn. Magn. Mater.* **2016**. [[CrossRef](#)]
22. Dar, A.A.; Elangovan, K. Influence of an inclined magnetic field and rotation on the peristaltic flow of a micropolar fluid in an inclined channel. *New J. Sci.* **2016**, 5717542. [[CrossRef](#)]
23. Abbas, Z.; Hasnaina, J.; Sajid, M. Hydromagnetic mixed convective two-phase flow of couple stress and viscous fluids in an inclined channel. *Z. Naturforsch.* **2014**, *69a*, 553–561. [[CrossRef](#)]
24. Lerisson, G.; Ledda, P.G.; Balestra, G.; Gallaire, F. Instability of a thin viscous film flowing under an inclined substrate: Steady patterns. *J. Fluid Mech.* **2020**, *898*, A6. [[CrossRef](#)]
25. Turkyilmazoglu, M. Nanofluid film flow due to a moving substrate and heat transfer. *Eur. Phys. J. Plus* **2020**, *135*, 1–13. [[CrossRef](#)]
26. Adesanya, S.O.; Egere, A.C.; Ukaegbu, J.C.; Lebelo, R.S. Influence of temperature-dependent properties on a gravity-driven thin film along inclined plate. *Nonlinear Eng.* **2020**, *9*, 118–123. [[CrossRef](#)]
27. Vaddemani, R.R.; Kodi, R.; Mopuri, O. Characteristics of MHD Casson fluid past an inclined vertical porous plate. *Mater. Today Proc.* **2022**, *49 Pt 5*, 2136–2142. [[CrossRef](#)]
28. Hafeez, N.M.; Abd-Alla, A.M.; Metwaly, T.M.N. Influences of rotation and mass and heat transfer on MHD peristaltic transport of Casson fluid through inclined plane. *Alex. Eng. J.* **2023**, *68*, 665–692. [[CrossRef](#)]
29. Mopuri, O.; Sailakumari, A.; Ganjikunta, A.; Sudhakara, E.; VenkateswaraRajus, K.; Ramesh, P.; Ganteda, C.; Reddy, B.R.; Varma, S.V.K. Characteristics of MHD Jeffery fluid past an inclined vertical porous plate. *CFD Lett.* **2024**, *16*, 68–89. [[CrossRef](#)]
30. Adesanya, S.O.; Souayah, B.; Rahimi-Gorji, M.; Khan, M.N.; Adeyemi, O.G. Heat irreversibility analysis for a couple stress fluid flow in an inclined channel with isothermal boundaries. *J. Taiwan Inst. Chem. Eng.* **2019**, *101*, 251–258. [[CrossRef](#)]
31. Abbas, Z.; Rafiq, M.Y.; Alshomrani, A.S.; Ullah, M.Z. Analysis of entropy generation on peristaltic phenomena of MHD slip flow of viscous fluid in a diverging tube. *Case Stud. Therm. Eng.* **2021**, *23*, 100817. [[CrossRef](#)]
32. Naz, R.; Noor, M.; Shah, Z.; Sohail, M.; Kumam, P.; Thounthong, P. Entropy generation optimization in MHD pseudoplastic fluid comprising motile microorganisms with stratification effect. *Alex. Eng. J.* **2020**, *59*, 485–496. [[CrossRef](#)]
33. Jha, B.K.; Yusuf, T.S. Entropy generation in an inclined porous channel with suction/injection. *Nonlinear Eng.* **2020**, *9*, 94–101. [[CrossRef](#)]
34. Khalid, A.; Khan, I.; Khan, A.; Shafie, S. Unsteady MHD free convection flow of Casson fluid past over an oscillating vertical plate embedded in a porous medium. *Eng. Sci. Technol. Int. J.* **2015**, *18*, 309–317. [[CrossRef](#)]
35. Awais, M.; Raja, M.A.Z.; Awan, S.E.; Shoaib, M.; Ali, H.M. Heat and mass transfer phenomenon for the dynamics of Casson fluid through porous medium over shrinking wall subject to Lorentz force and heat source/sink. *Alex. Eng. J.* **2021**, *60*, 1355–1363. [[CrossRef](#)]
36. Prameela, M.; Gangadhar, K.; Reddy, G.J. MHD free convective non-Newtonian Casson fluid flow over an oscillating vertical plate. *Partial Differ. Equ. Appl. Math.* **2022**, *5*, 100366. [[CrossRef](#)]
37. Vishalakshi, A.B.; Mahabaleswar, U.S.; Ahmad, M.H.; Sharifpur, M. An MHD Casson fluid flow past a porous stretching sheet with threshold Non-Fourier heat flux model. *Alex. Eng. J.* **2023**, *69*, 727–737. [[CrossRef](#)]
38. Adel, M.; Khader, M.M.; Ahmad, H. MHD nanofluid flow and heat transfer caused by a stretching sheet that is heated convectively: An approximate solution using ADM. *Case Stud. Therm. Eng.* **2024**, *60*, 104683. [[CrossRef](#)]

**Disclaimer/Publisher’s Note:** The statements, opinions and data contained in all publications are solely those of the individual author(s) and contributor(s) and not of MDPI and/or the editor(s). MDPI and/or the editor(s) disclaim responsibility for any injury to people or property resulting from any ideas, methods, instructions or products referred to in the content.